

# A cortical motor nucleus drives the basal ganglia-recipient thalamus in singing birds

Jesse H Goldberg & Michale S Fee

The pallido-recipient thalamus transmits information from the basal ganglia to the cortex and is critical for motor initiation and learning. Thalamic activity is strongly inhibited by pallidal inputs from the basal ganglia, but the role of nonpallidal inputs, such as excitatory inputs from cortex, remains unclear. We simultaneously recorded from presynaptic pallidal axon terminals and postsynaptic thalamocortical neurons in a basal ganglia-recipient thalamic nucleus that is necessary for vocal variability and learning in zebra finches. We found that song-locked rate modulations in the thalamus could not be explained by pallidal inputs alone and persisted following pallidal lesion. Instead, thalamic activity was likely driven by inputs from a motor cortical nucleus that is also necessary for singing. These findings suggest a role for cortical inputs to the pallido-recipient thalamus in driving premotor signals that are important for exploratory behavior and learning.

Basal ganglia thalamocortical circuits are evolutionarily conserved among vertebrates and have been widely implicated in motor control and learning<sup>1,2</sup>. The major output of the basal ganglia circuit, pallidal neurons that are GABAergic and tonically active, are thought to control movements by inhibiting or disinhibiting their targets in the pallido-recipient thalamus<sup>3–5</sup>. This thalamic area also receives excitatory inputs from cortex<sup>6</sup>, but thalamic integration of cortical and pallidal inputs is poorly understood. In human disease, the pallidal inputs are often emphasized: insufficient pallidal inhibition of thalamus is thought to result in hyperkinesias such as dystonia, and excess inhibition can result in hypokinesias such as Parkinson's disease<sup>5,7</sup>. During normal behavior, however, premotor signals in primate thalamus are not easily explained by pallidal inputs alone<sup>8,9</sup> and even persist following pallidal inactivation<sup>10</sup>, leading to some question about the origins of activity in pallido-recipient thalamic areas<sup>11–13</sup>.

Songbirds offer a tractable model system for studying the origins of neural activity in motor thalamus. The vocal portion of the songbird basal ganglia-recipient thalamic nucleus DLM (dorsolateral division of the medial thalamus) is part of a premotor thalamocortical circuit that is essential for song learning (Fig. 1a,b)<sup>14,15</sup>. Lesions to DLM or its target, the frontal cortical nucleus LMAN (lateral magnocellular nucleus of the anterior nidopallium), abolish vocal babbling and variability in juvenile birds<sup>16,17</sup>. Because the pallidal projection to DLM terminates at a presynaptic terminal that is large enough to be recorded extracellularly (Fig. 1c), songbirds provide an opportunity to simultaneously record from a thalamic neuron and its presynaptic pallidal input<sup>18–20</sup>.

To investigate the origins of thalamic activity during behavior, we recorded from antidromically identified thalamocortical neurons and their pallidal and cortical inputs in singing juvenile birds. Premotor signals in DLM were not easily explained by pallidal inputs alone and persisted following pallidal lesion. Instead, our findings support the idea that descending cortical inputs drive song-locked rate modulations

in basal ganglia-recipient thalamus<sup>10,12</sup> and support a role for the thalamus in linking distinct cortical motor areas that are important for exploratory behavior during learning<sup>21</sup>.

## RESULTS

### Thalamic neurons are activated during singing

To understand the role of the thalamus in song production, we recorded from neurons in the vocal portion of DLM in freely behaving juvenile zebra finches<sup>22</sup> (Fig. 1c,d and Supplementary Figs. 1 and 2, see Online Methods). Many of these neurons were antidromically identified as thalamocortical neurons projecting to LMAN ( $n = 17$  of 29; Online Methods). The other 12 neurons did not respond to LMAN stimulation with a short-latency spike, but did exhibit spike waveforms, firing patterns and correlations to song temporal structure similar to those of the identified projection neurons and were included in the analysis. Although DLM neurons recorded in anesthetized birds discharge at very low rates ( $<10$  Hz)<sup>18–20</sup>, they exhibited high average firing rates in awake birds and were further activated during singing (singing,  $89.0 \pm 39.7$  Hz; non-singing,  $60.7 \pm 30.4$  Hz;  $P < 0.001$ , paired  $t$  test,  $n = 25$  of 29, 11 birds, mean  $\pm$  s.e.m.; Fig. 1d). Thalamic neurons also exhibited increased peak firing rates during singing (95<sup>th</sup> percentile rate,  $394.4 \pm 26.8$  Hz versus  $196.9 \pm 13.8$  Hz,  $n = 29$  of 29 neurons,  $P < 0.001$ , paired  $t$  tests). These periods of high-frequency firing (Fig. 1d,e) differed from low threshold bursts that were previously observed in mammalian thalamic neurons during low arousal states<sup>23</sup> and in DLM neurons in anesthetized birds<sup>18–20</sup>. Two common criteria for low threshold bursts are burst refractory periods ( $>50$  ms) and a period of quiescence ( $>50$  ms) before burst onset<sup>24</sup>. We did not observe thalamic discharge events that met these criteria. Instead, brief periods of high tonic discharge (HTD), defined as firing events greater than 250 Hz (Online Methods), were generated from high background firing rates ( $>100$  Hz) and did not exhibit refractory

McGovern Institute for Brain Research, Department of Brain and Cognitive Sciences, Massachusetts Institute of Technology, Cambridge, Massachusetts, USA. Correspondence should be addressed to M.S.F. (fee@mit.edu).

Received 26 September 2011; accepted 12 January 2012; published online 12 February 2012; doi:10.1038/nn.3047

**Figure 1** Firing patterns of thalamic neurons and their pallidal inputs during singing. **(a,b)** LMAN, Area X and DLM constitute cortical<sup>48</sup>, basal ganglia (BG) and thalamic portions of the song system, respectively. LMAN contributes to vocal output through its projection to RA, a motor cortical (MC) nucleus, which in turn projects to brainstem motor neurons. Adult song production involves the HVC to RA projection. **(c)** Confocal image of a calyceal pallidal axon terminal (red) and the postsynaptic DLM neuron (green). **(d)** Extracellular voltage trace and the instantaneous firing rate of a single thalamic neuron recorded during subsong (spectrogram shown above, 44 dph). Asterisks indicate examples of HTD events. Inset, antidromic identification and collision testing demonstrating the projection to LMAN; evoked DLM spike following stimulation in LMAN (black trace), LMAN stimulation triggered by a spontaneously DLM elicited no antidromic spike (red trace). Vertical and horizontal scale bars represent 1 mV and 1 ms, respectively. **(e)** Expanded view from **d** (gray bar). **(f)** Syllable onset-aligned rate histograms for the neuron shown in **d** (top) and an average of all DLM neurons (bottom, shading indicates  $\pm$  s.e.m.;  $n = 14$ ). **(g)** Syllable offset-aligned rate histogram. Data are shown as in **f**. **(h-k)** Data are plotted as in **d-g** for a pallidal axon terminal recorded in the same bird and on the same day as the DLM neuron from **d**.

periods (**Supplementary Fig. 1**). HTD events were more common during singing than during awake, non-singing periods (singing,  $11.2 \pm 1.3$  HTDs  $s^{-1}$ ; non-singing,  $2.4 \pm 0.8$  HTDs  $s^{-1}$ ;  $n = 28/29$  neurons,  $P < 0.001$ , paired  $t$  test, Online Methods).

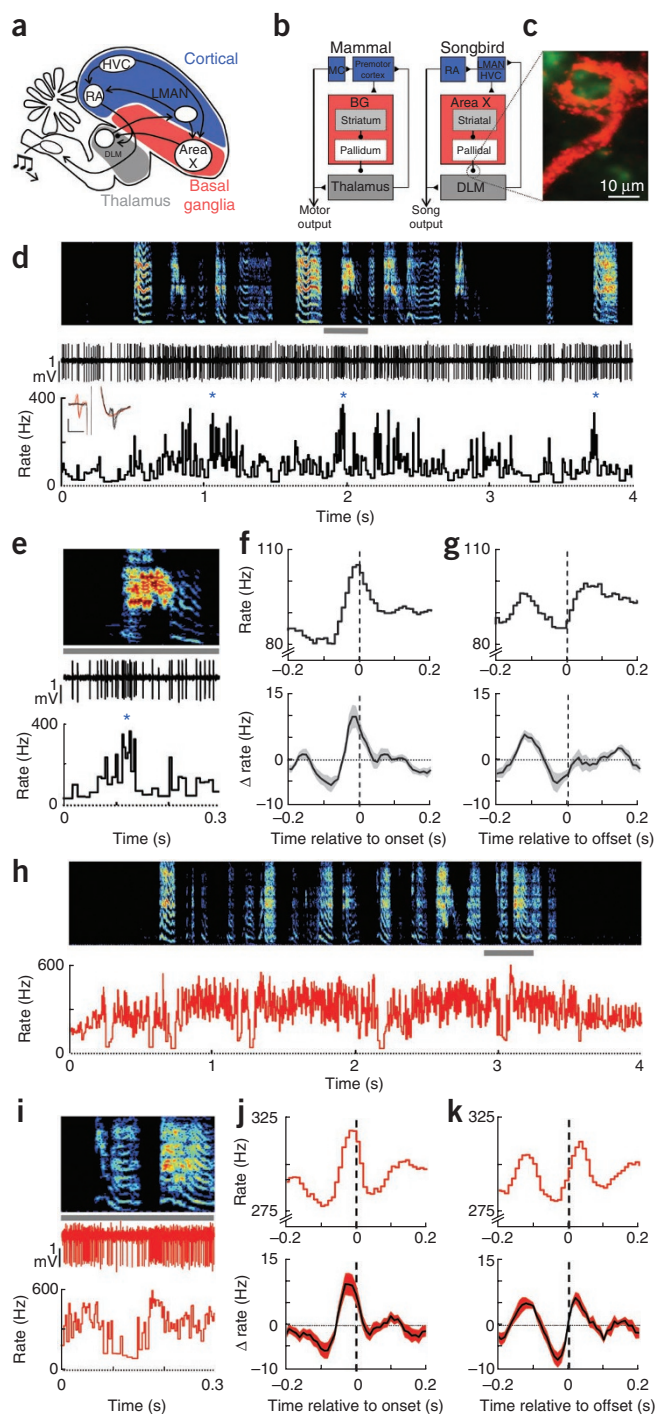
We examined the temporal relation between DLM activity and song vocalizations. In the youngest birds (<45 d post hatch, dph), which generate subsong (highly random vocalizations akin to babbling), almost all DLM neurons were strongly activated at syllable onsets, exhibiting an average rate increase of  $13.5 \pm 1.9$  Hz that began  $27.1 \pm 6.2$  ms before syllable onsets ( $P < 0.05$  in 13 of 14 cells; **Fig. 1e,f** and Online Methods). Prior to syllable offsets, most DLM neurons were briefly suppressed by an average of  $8.2 \pm 1.2$  Hz ( $P < 0.05$  in  $n = 11$  of 14 cells), and this suppression began  $40.0 \pm 9.1$  ms before syllable offsets (**Fig. 1g**). Given that DLM lesions abolish vocal babbling<sup>17</sup>, these rate modulations could be involved in driving the initiation and termination of syllables in early song vocalizations.

After the subsong stage (>45 dph), juvenile birds begin singing ‘plastic’ song, which contains distinct, identifiable syllables of relatively fixed duration<sup>25,26</sup>. All DLM neurons recorded at this stage exhibited song-locked rate modulations, but the timing of these modulations was much less homogeneous than in subsong birds. Specifically, in plastic song birds, a given DLM neuron could exhibit peaks or dips at various times in syllable-aligned rate histograms, although there was a trend for neurons to exhibit peaks before syllable onsets ( $n = 7$  of 15) and dips before syllable offsets ( $n = 7$  of 15) (**Supplementary Fig. 2**).

### Pallidal inputs to thalamus are activated during singing

We next set out to determine the origins of the homogenous syllable-locked signals observed in DLM of subsong birds. In both songbirds and mammals, thalamic rate increases can be facilitated by pauses in the spiking of inhibitory pallidal inputs<sup>4,19</sup>. Thus, we hypothesized that pallidal inputs to DLM would exhibit average firing-rate modulations opposite those of DLM neurons, that is, rate suppression before syllable onsets and activation before syllable offsets. To test this hypothesis, we recorded from the calyceal pallidal axon terminals that form 1:1 synaptic contacts with DLM neurons<sup>18–20,27</sup> during singing. We also recorded from the cell bodies (in the basal ganglia homolog Area X) of putative DLM-projecting pallidal neurons that give rise to the pallidal terminals in DLM ( $n = 17$  cells, 4 birds; **Supplementary Fig. 3**)<sup>18,22</sup>.

Notably, pallidal inputs also exhibited increased average firing rates during subsong (non-singing,  $144.4 \pm 27.8$  Hz; singing,  $296.0 \pm 14.4$  Hz;



$P < 0.001$ , paired tests,  $n = 14$  of 14 terminals; **Fig. 1h**), as well as a peak in firing rate before subsong syllable onsets (rate increase of  $17.1 \pm 2.4$  Hz, beginning  $41.4 \pm 2.6$  ms before onsets,  $P < 0.05$  in 12 of 14 terminals; **Fig. 1i,j**), and a decrease in firing rate before syllable offsets (rate decrease of  $7.0 \pm 2.3$  Hz, beginning  $51.4 \pm 8.0$  ms before offsets,  $P < 0.05$  in 8 of 14 terminals; **Fig. 1k**). Contrary to what would be expected if thalamic signals were simply inverting pallidal inputs, no pallidal axon terminals recorded in DLM or pallidal cell bodies recorded in Area X (**Supplementary Fig. 2**) exhibited either an average firing rate decrease before subsong syllable onsets or a firing rate increase before subsong syllable offsets.

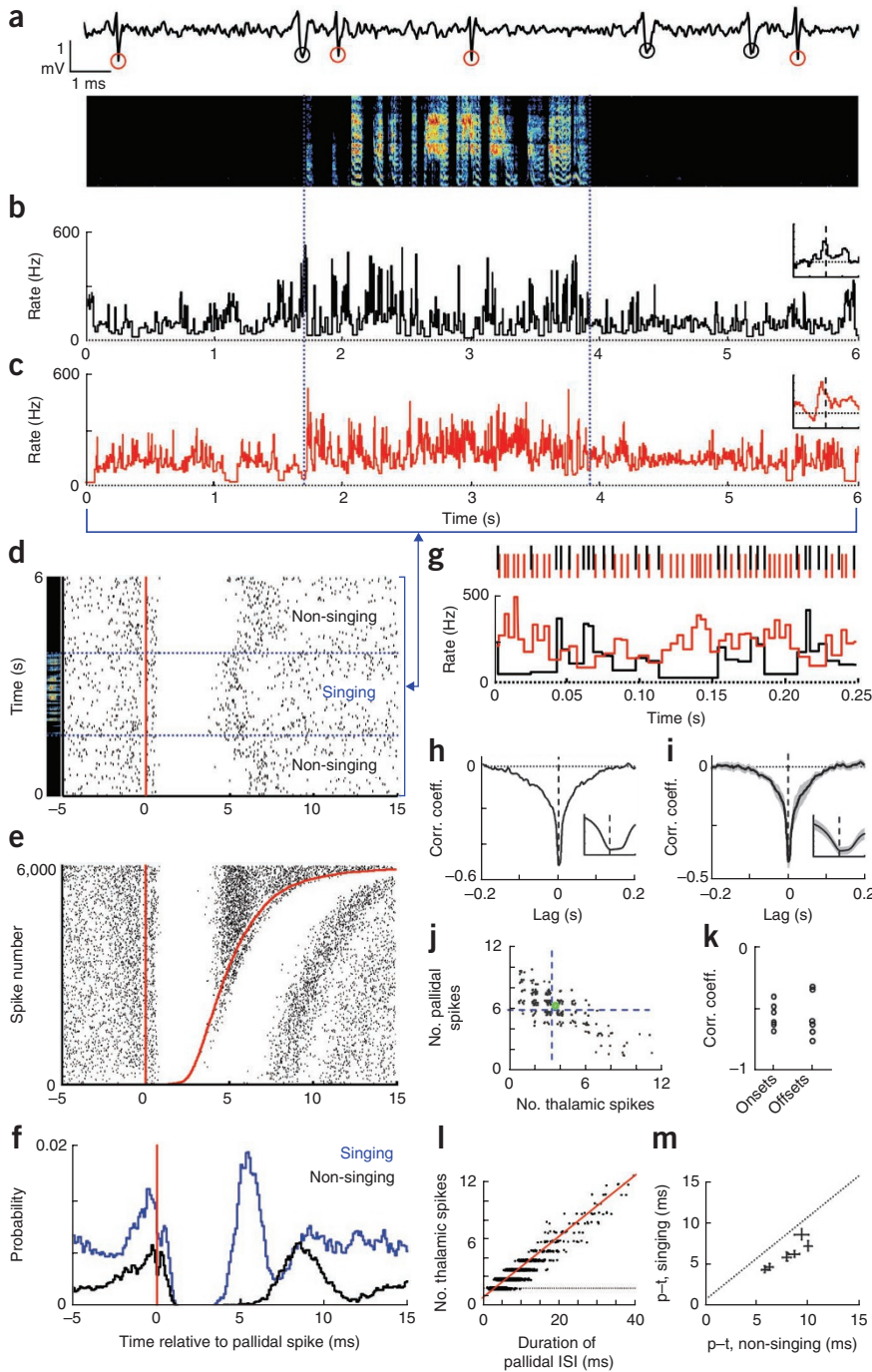


**Figure 2** Simultaneous recordings of pallidal axon terminal and putative post-synaptic thalamic neurons during singing. **(a)** Extracellular waveform containing thalamic and pallidal spikes (black and red circles, respectively). **(b,c)** Instantaneous firing rates of the thalamic and pallidal neurons during subsong (spectrogram above, 48 dph). Insets, syllable onset-aligned rate histograms, plotted as in **Figure 1g** (*x* axis,  $\pm 0.2$  s relative to syllable onset; *y* axis,  $\Delta$  rate:  $-10$  to  $25$  Hz). **(d)** Raster plot of thalamic spikes (black ticks) aligned to the timing of pallidal spikes (red line) for the data shown in **b** and **c**. **(e)** Raster plot, as in **d**, sorted by the duration of the pallidal ISI during singing. Red line at the right shows the time of the next pallidal spike (6,000 pallidal ISIs shown). **(f)** Histograms of thalamic spike probability relative to pallidal spike times. **(g)** Magnification of **b** and **c** (\*), showing anti-correlation of pallidal (red) and thalamic (black) IFRs. **(h)** Lag cross-correlation of the firing rates (same pair). Inset, expanded view of the negative peak of the cross correlation ( $\pm 10$  ms). **(i)** Average lag cross-correlation of six pairs (shading,  $\pm$  s.e.m.). **(j)** Scatter plot of the number of pallidal spikes versus thalamic spikes that occurred in a 30-ms window before each syllable onset (255 syllables, same pair as shown in **b** and **c**). Green circle indicates mean number of spikes in this window. Blue dashed lines indicate average number of pallidal and thalamic spikes in random 30-ms windows during singing. **(k)** Correlation, for all six pairs, between the number of pallidal and thalamic spikes occurring in the 30 ms preceding syllable onsets and offsets. **(l)** The number of thalamic spikes within each pallidal ISI, plotted as a function of ISI duration (red line, linear regression; pair from **b** and **c**). **(m)** The duration of thalamic spike suppression, measured as the average latency from the pallidal spike to the following thalamic spike (*p*-*t*), during singing plotted versus non-singing ( $\pm$  s.d.,  $n = 6$  pairs).

### Coactivation of connected pallidal and thalamic neurons

These results raise several important questions. First, how do thalamic neurons discharge at high rates ( $\sim 100$  Hz) in the face of highly active pallidal inputs ( $\sim 300$  Hz)? One possibility is that the pallidal inputs are not as strongly inhibitory as was previously believed<sup>27</sup>. To test this possibility, we recorded simultaneously from LMAN-projecting DLM neurons, together with the putative presynaptic axon terminal, at the end of the same electrode<sup>18–20</sup> in awake behaving birds ( $n = 7$  pairs total, 5 pairs in juvenile birds, 4 of which were recorded during singing, and an additional 2 pairs in singing adults; **Fig. 2** and **Supplementary Figs. 4–6**, see Online Methods). In all of the pairs, the pallidothalamic interaction was indeed strongly inhibitory; thus, results from both adults and juveniles were pooled in the following analysis (**Supplementary Fig. 5**).

Rasters of thalamic spikes, aligned to simultaneously recorded pallidal spikes, revealed that each pallidal spike was followed by a period of absolute thalamic spike suppression (**Fig. 2d,e**), similar to what is observed in pairs recorded in anesthetized birds<sup>18–20</sup>. However, the duration of this suppression, measured as the latency from each pallidal spike to the following thalamic spike, was extremely brief during singing ( $5.2 \pm 0.6$  ms,  $n = 6$  pairs), substantially shorter than was previously observed under anesthesia ( $\sim 20$  ms)<sup>18–20</sup>. Following this suppression, thalamic neurons spiked with a high probability in a narrow time window, resulting in a large, narrow peak in the pallido-thalamic cross-correlogram (**Fig. 2f** and **Supplementary Fig. 5**). During singing, the standard deviation of this peak was extremely small ( $0.82 \pm 0.2$  ms,  $n = 6$  pairs during singing), indicating that the first thalamic spike that occurred in a pallidal interspike interval was locked to the preceding pallidal spike with submillisecond precision.

Although pallidal inputs were strongly inhibitory, thalamic spiking was not restricted to pallidal pauses. The duration of DLM spike suppression (5–95% range,  $3.9 \pm 0.5$ – $6.9 \pm 0.9$  ms;  $n = 6$  pairs) was well within the distribution of the simultaneously recorded pallidal



interspike intervals (mean,  $4.0 \pm 0.5$  ms; 5–95% range,  $2.2 \pm 0.2$ – $7.2 \pm 1.1$  ms,  $n = 6$  pairs; **Fig. 2e–g** and **Supplementary Fig. 5**). Across all pairs, one or more thalamic spikes occurred in  $23.1 \pm 8.8\%$  of pallidal interspike intervals (ISIs) during singing. Notably, thalamic neurons spiked sooner after the preceding pallidal spike during singing than during non-singing periods (non-singing,  $8.0 \pm 0.7$  ms; singing,  $5.2 \pm 0.6$  ms;  $P < 0.001$  in 6 of 6 pairs), enabling thalamic neurons to discharge at rates in excess of  $\sim 100$  Hz during singing even in the presence of powerfully inhibitory inputs occurring at  $\sim 300$  Hz (**Fig. 2**). In summary, thalamic neurons were able to discharge at high rates during singing because each pulse of pallidal inhibition was so brief.

We wondered whether this brief, millisecond-timescale inhibition exerted by pallidal inputs had a net suppressive effect on thalamic firing rates on broader timescales or whether it might instead effectively increase thalamic firing rates, for example by the post-inhibitory rebound mechanism observed under anesthesia<sup>18</sup>. Pallidal suppression of thalamic firing rate was visibly apparent in the simultaneously recorded spike trains (**Fig. 2g** and **Supplementary Fig. 7**). The suppression of thalamic spikes by pallidal spikes was quantified with a standard spike train cross-correlation analysis in large (10 ms) time bins (**Supplementary Fig. 6g**), as well as the cross-correlation between pallidal and thalamic instantaneous firing rates (IFRs) during singing (median width at half-minimum,  $19.4 \pm 10.6$  ms; zero lag cross-correlation,  $-0.44 \pm 0.04$ ;  $P < 0.01$ ,  $n = 6$  of 6 pairs; **Fig. 2h,i** and Online Methods). Both of these analyses confirmed that pallidal and thalamic firing rates were significantly anti-correlated and that, on average, pallidal rate increases were associated with thalamic rate decreases and vice versa.

If the pallidothalamic interaction is inhibitory, how do both pallidal and thalamic neurons exhibit the same syllable-locked changes in firing rate? We tested whether pallidal inputs were also inhibitory at syllable onsets and offsets. In the paired recordings, we plotted the number of pallidal spikes that occurred in the 30 ms before each syllable onset against the number of thalamic spikes that occurred in the same period and found that they were strongly anti-correlated in all pairs. Rate changes before syllable offsets were also anti-correlated (onsets,  $-0.61 \pm 0.04$ ; offsets,  $-0.62 \pm 0.07$ ;  $P < 0.001$ ,  $n = 6$  of 6 pairs; **Fig. 2j,k**). Together, these findings demonstrate that increases in pallidal firing rate were associated with a suppression of thalamic spiking, even at syllable onsets and offsets.

Pallidal suppression of thalamic spiking was also evident in single pallidal ISIs. The number of thalamic spikes that discharged in a single pallidal ISI was strongly linearly dependent on the duration of that ISI ( $r = 0.80 \pm 0.05$ ,  $n = 6$  pairs during singing). That is, longer pallidal ISIs contained more thalamic spikes, consistent with previous observations in anesthetized birds (**Fig. 2l**)<sup>19</sup>. During singing, the first thalamic spike occurred, on average,  $5.2 \pm 0.6$  ms after a pallidal spike, and an additional

thalamic spike discharged for every  $3.9 \pm 0.6$  ms increase in the duration of the pallidal ISI (data are mean  $\pm$  s.e.m. for six pairs during singing). We used this empirical relation between pallidal ISI and thalamic spiking to predict thalamic spiking in response to each pallidal spike train recorded during subsong (**Supplementary Fig. 8**). Consistent with the result that pallidal inputs suppressed thalamic spiking (**Fig. 2g–i**), simulated thalamic activity exhibited rate decreases before syllable onsets and rate increases before offsets (**Supplementary Fig. 8**), exactly the opposite of what was actually observed. Together, these findings suggest that pallidal inputs did not drive the thalamic rate changes that we observed at subsong syllable onsets and offsets (**Fig. 1g,h**).

### Activation of thalamic neurons in Area X-lesioned birds

We hypothesized that song-locked thalamic firing patterns might be driven by non-pallidal inputs. If this is true, then DLM neurons should exhibit these modulations even after removal of pallidal inputs. To test this possibility, we recorded LMAN-projecting DLM neurons in Area X-lesioned birds ( $n = 3$  birds; **Fig. 3a,b** and Online Methods). As in intact birds, DLM neurons in lesioned birds were more active during singing than during non-singing, exhibiting higher average firing rates (non-singing,  $25.6 \pm 14.7$  Hz; singing,  $58.6 \pm 23.6$  Hz;  $P < 0.05$ , paired  $t$  test,  $n = 6$  of 6 neurons; **Fig. 3c**).

DLM neurons in Area X-lesioned birds also exhibited the same song-locked rate modulations that we observed in intact birds (**Fig. 3d–f**). They showed increased firing rates at syllable onsets (average  $20.0 \pm 5.1$  Hz increase starting  $40.0 \pm 6.8$  ms before onsets,  $P < 0.05$  in 6 of 6 cells) and decreased firing rates before syllable offsets (average  $13.0 \pm 2.6$  Hz decrease starting  $26.0 \pm 12.1$  ms before offsets,  $P < 0.05$ , 5 of 6 cells). Thus, song-locked rate modulations in DLM did not require pallidal inputs, suggesting that other inputs to the thalamus are involved.

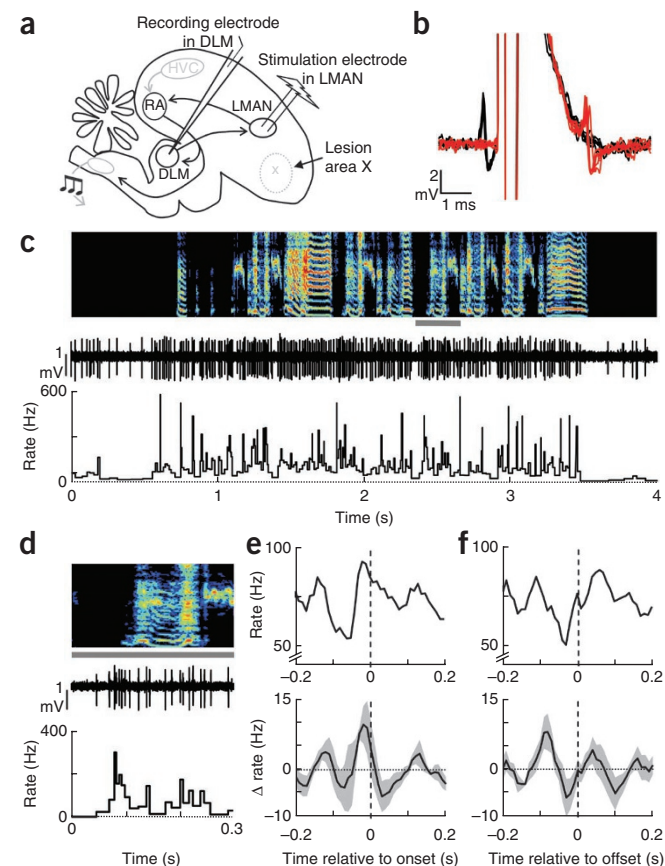


**Figure 3** Song-locked rate modulations in thalamic neurons are also observed after basal ganglia lesions. **(a)** Schematic of experimental design of recording and stimulation electrodes in DLM and LMAN, and of lesion of Area X (see Online Methods). **(b)** Antidromic identification and collision testing of an LMAN-projecting neuron in DLM. **(c)** Extracellular voltage trace and instantaneous firing rate of the same DLM neuron (shown in **b**) recorded during singing (spectrogram shown above). **(d)** Example of spiking of the DLM neuron at a syllable onset. Data are an expanded view from the period marked by a gray bar in **c**. **(e)** Syllable onset-aligned rate histograms for the same neuron (top), and for all DLM neurons recorded in Area X-lesioned birds (bottom,  $n = 6$  neurons from 3 birds). Note that the apparent rate change in the population histogram was less than that measured across neurons because the peak before syllable onsets occurred at slightly different times in different neurons. **(f)** Syllable offset aligned rate histograms; data are presented as in **e**.

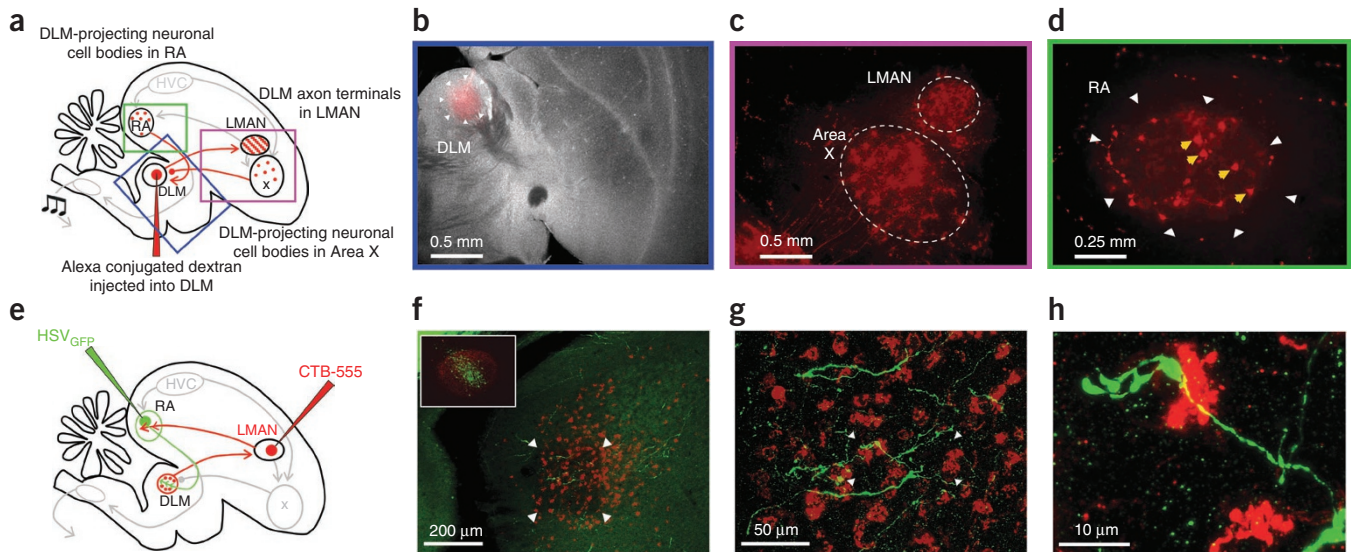


**Figure 4** Anatomical verification of the RA projection to DLM in juvenile birds. **(a)** Schematic of retrograde identification of DLM-projecting RA neurons. Boxes highlight expanded views shown in **b–d**. **(b)** Merged darkfield fluorescence section showing Alexa-555-conjugated dextran injected into the vocal portion of DLM in a juvenile bird (37 dph). **(c)** Retrograde labeling of cell bodies in Area X and axon terminals in LMAN, confirming the placement of tracer into the vocal portion of DLM. **(d)** Following injection of tracer into DLM, cell bodies were also labeled in RA (yellow arrows). **(e)** Schematic of anterograde identification of RA axon terminals in DLM. **(f)** Micrograph of DLM showing neurons retrogradely labeled (red) by injection of tracer into LMAN. RA axon terminals (green) were labeled by injection of GFP-expressing herpes virus into RA. Inset, micrograph of RA showing anterograde label of LMAN axon terminals (red) and GFP-expressing neurons (green). **(g)** Expanded view micrograph in DLM showing RA terminals from the region marked by the arrowheads in **f**. **(h)** Expanded view of the region marked by the arrowheads in **g**.

### A corticothalamic projection drives thalamic spiking *in vivo*

What, then, gives rise to the three aspects of subsong-related firing rate modulations observed in thalamic neurons: overall activation during singing, rate increases before syllable onsets and rate decreases before syllable offsets? To identify non-pallidal inputs to DLM, we injected retrograde tracer into DLM and observed labeling of a subpopulation of neurons in the motor cortical nucleus RA (robust nucleus of the arcopallium,  $n = 3$  birds; **Fig. 4a–d** and Online Methods), consistent with previous reports<sup>28,29</sup>. Furthermore, injections of a virus expressing green fluorescent protein (GFP) into RA revealed extensive axonal terminations in the LMAN-projecting part of DLM ( $n = 3$  of 3 birds; **Fig. 4e–h** and **Supplementary Fig. 9**). This presumably glutamatergic projection<sup>28</sup> is analogous to corticothalamic pathways found in mammals (**Fig. 1b**)<sup>6,21</sup>.

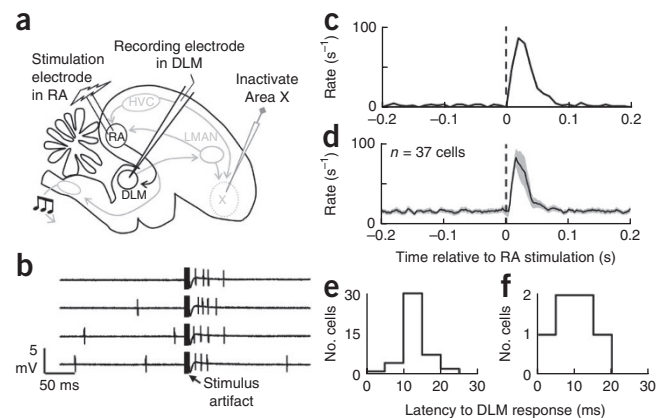
To test whether the descending projection from RA could drive spiking in DLM, we recorded DLM neurons in anesthetized juvenile birds during electrical stimulation of RA (see Online Methods). Because stimulation in RA could potentially influence DLM through Area X (by antidromic activation of HVC and LMAN), Area X was inactivated during these experiments (**Fig. 5a** and **Supplementary Figs. 10** and **11**, see Online Methods). RA stimulation strongly

activated DLM neurons, causing a significant increase in firing rate (average rate increase =  $106.0 \pm 17.3$  Hz,  $P < 0.01$  in 37 of 39 neurons,  $n = 9$  birds; **Fig. 5b–d** and **Supplementary Fig. 10**, see Online Methods) at low latencies ( $12.6 \pm 0.8$  ms,  $n = 37$  neurons; **Fig. 5e,f**). These findings demonstrate the functionality and excitatory nature of the corticothalamic projection from RA to DLM.

### Cortical inputs to thalamus are activated during singing

To further examine the idea that syllable-related thalamic rate modulations are driven by these cortical inputs, we recorded antidromically identified neurons in RA that project to DLM (RA<sub>DLM</sub> neurons) in singing juvenile birds (**Fig. 6a–d**). Of 115 neurons recorded in RA of five subsong birds, 17 were antidromically identified as projecting to DLM. RA<sub>DLM</sub> neurons exhibited notably homogenous firing patterns. All neurons showed increased average firing rates during singing (non-singing,  $18.2 \pm 2.2$  Hz; singing,  $44.2 \pm 7.7$ ;  $P < 0.001$ , paired  $t$  test). All of the neurons also showed a peak in firing rate before syllable onsets

**Figure 5** RA stimulation activates DLM neurons. **(a)** Schematic of the experimental design. DLM neurons were recorded in anesthetized birds during inactivation of Area X<sup>19</sup> (see **Supplementary Fig. 10**). **(b)** Four example traces of a DLM neuron recorded during burst stimulation of RA (five stimulations at 500 Hz). Note the increase in DLM firing rate immediately following RA stimulation. Single-pulse stimulation of RA was also effective in driving DLM neurons (see **Supplementary Fig. 10**). **(c)** RA stimulation-aligned rate histogram for the neuron shown in **b**. **(d)** Average peristimulus histogram for 37 neurons recorded in nine birds (shading indicates  $\pm$  s.e.m.). **(e)** Histogram of response latencies of DLM neurons following RA burst stimulation ( $n = 37$  neurons). **(f)** Histogram of response latencies in DLM following single-pulse stimulation in RA.





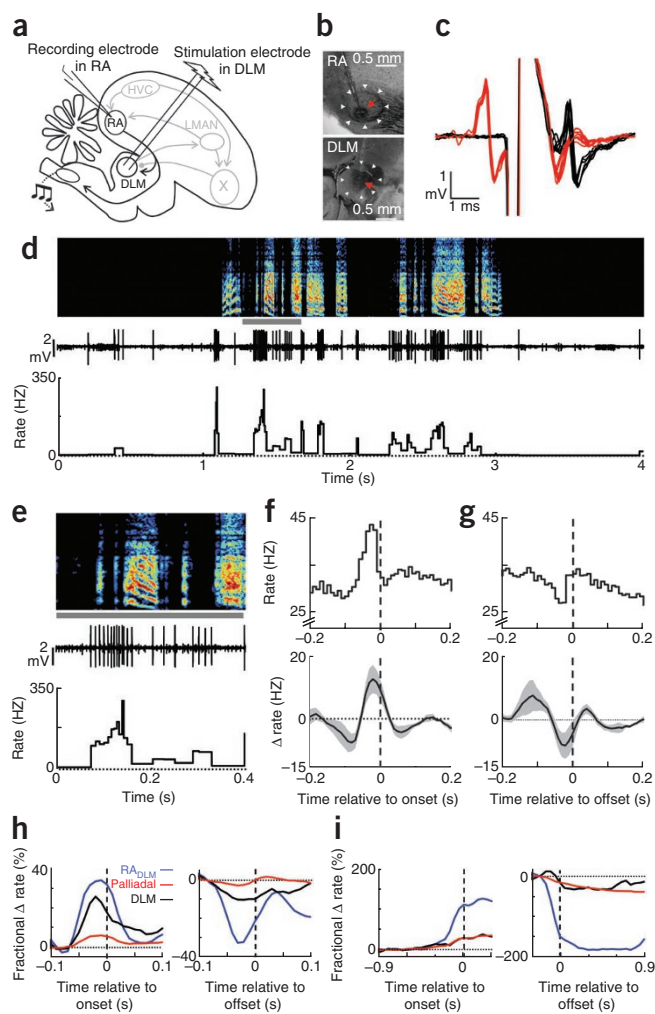


**Figure 6** Singing-related firing patterns of corticothalamic RA neurons projecting to DLM. **(a)** Schematic of experimental design. **(b)** Histological verification of recording and stimulation electrodes in RA and DLM. **(c)** Antidromic identification and collision testing of a DLM-projecting neuron in RA. **(d)** Extracellular voltage trace and instantaneous firing rate of the same RA<sub>DLM</sub> neuron (shown in **c**) recorded during singing (spectrogram shown above, 46 dph). **(e)** Example of spiking of an RA<sub>DLM</sub> neuron at syllable onsets from the period marked by a gray bar in **d**. **(f)** Syllable onset-aligned rate histograms for the same neuron (top) and average of all RA<sub>DLM</sub> neurons (bottom,  $n = 17$ ). **(g)** Syllable offset-aligned rate histograms; data are presented as in **g**. **(h)** Average fractional rate change ( $\Delta$  rate divided by the mean baseline rate) for RA<sub>DLM</sub> neurons ( $n = 17$ , blue), pallidal terminals ( $n = 14$ , red) and DLM neurons ( $n = 14$ , black) aligned to syllable onsets (left) and offsets (right). **(i)** Average fractional rate changes, plotted as in **h**, aligned to the onset of singing (left) and offset of singing (right).

(rate increase of  $21.0 \pm 4.8$  Hz,  $P < 0.05$  in 17 of 17 cells; **Fig. 6e,f**), and most of the neurons exhibited a decrease in firing rate before syllable offsets (rate decrease of  $13.0 \pm 4.4$  Hz,  $P < 0.05$  in 15 of 17 cells; **Fig. 6g**). In contrast, neurons not identified as DLM projectors exhibited a range of different firing patterns (**Supplementary Fig. 12**). Notably, the rate increase at syllable onsets occurred significantly earlier in RA<sub>DLM</sub> neurons than in DLM neurons (RA<sub>DLM</sub>,  $43.7 \pm 4.5$  ms; DLM,  $27.1 \pm 6.2$  ms;  $P < 0.05$ ,  $t$  test; **Fig. 6h**) and trended to earlier times for the rate decrease before syllable offsets (RA<sub>DLM</sub>,  $48.2 \pm 6.2$  ms; DLM,  $40.0 \pm 9.1$  ms;  $P > 0.2$ ). Thus, both the amplitude and the timing of rate modulations in RA<sub>DLM</sub> neurons were consistent with a

role in driving thalamic activity during singing. Of course we cannot rule out the additional possible involvement of other, uncharacterized, inputs to DLM.

Examining the pallidal, thalamic and corticothalamic firing patterns side-by-side revealed that the excitatory cortical inputs to the thalamus were temporally matched by the inhibitory pallidal inputs at syllable onsets and offsets, as well as during the transitions into and out of singing (**Fig. 6h,i**). Although the timing of inhibitory and excitatory inputs was closely balanced, the relative magnitudes of the rate modulations, when normalized by the baseline firing rate, were significantly larger in RA<sub>DLM</sub> neurons than in both the pallidal inputs and the DLM neurons themselves ( $P < 0.01$  in  $t$  tests for all comparisons, see Online Methods). These large fractional changes in firing rate of the RA<sub>DLM</sub> neurons may explain how they were able to drive thalamic activity in the face of opposing inhibitory signals during singing.

## DISCUSSION

We examined the origins of neural activity in DLM, a basal ganglia-recipient thalamic nucleus that is necessary for vocal babbling in juvenile birds<sup>17</sup>. DLM neurons were strongly activated during singing and exhibited peaks in firing rate immediately before subsong syllable onsets. Paradoxically, pallidal inputs to DLM, although inhibitory, were also activated during singing and before syllable onsets. We hypothesized a role for non-pallidal inputs to DLM and found that song-locked thalamic rate modulations persisted following lesion of pallidal inputs. Furthermore, activation of cortical inputs to DLM from the motor nucleus RA drove DLM neurons *in vivo*. Consistent with a role in driving DLM signals during behavior, antidromically identified corticothalamic neurons were activated during singing and exhibited rate peaks before syllable onsets. Together, these findings suggest that cortical inputs can be the principle drivers of behavior-locked activity in the basal ganglia-recipient motor thalamus<sup>12</sup>.

Do our findings apply to mammalian basal ganglia-thalamocortical circuits? In mammals, the role of pallidal inhibition in controlling thalamic activation and the initiation of movement is widely recognized<sup>3–5</sup>. However, thalamic signals are not easily explained by pallidal inputs alone during behavior<sup>8,9,12</sup>. For example, in cued saccade or arm movement tasks in primates, most thalamic neurons exhibit a brisk peak in activity immediately before movement onset<sup>8,9,13</sup>, similar to the rate peak that we observed before syllable onsets. In contrast with what would be predicted if these signals were driven by pauses in pallidal activity<sup>4</sup>, most pallidal neurons in these tasks also exhibit rate increases at movement onset<sup>13,30–34</sup>, similar to the pallidal terminals that we observed.

At least two explanations have been put forward to reconcile paradoxical pallido-thalamic coactivations that have been observed during behavior. First, thalamic spiking might be driven directly by pallidal rate increases through a post-inhibitory rebound mechanism. In this model, increased pallidal activity hyperpolarizes thalamic neurons, causing de-inactivation of low threshold calcium channels. Following a brief pallidal pause, these calcium channels then trigger a rebound thalamic burst<sup>23,35</sup>. Rebound spiking is observed in DLM neurons in brain slices and in anesthetized songbirds<sup>18,20,36</sup>, where both pallidal axon terminals and connected thalamic neurons are coactivated during song playback or cortical stimulation<sup>18,20</sup>.

The rebound model does not easily fit with our results during singing. First, the calcium channels that drive rebound spikes rapidly inactivate at depolarized membrane potentials<sup>37</sup>. Thus, rebound spiking is associated with low levels of thalamic activation, such as during drowsiness, anesthesia or sleep<sup>23</sup>. Indeed, DLM neurons discharge at very low rates in anesthetized birds ( $<10$  Hz)<sup>18–20</sup>, more than an order

of magnitude lower than what we observed during singing (~100 Hz). Second, rebound bursts cause calcium channel inactivation<sup>23</sup> and are followed by substantial (>50 ms) burst refractory periods in DLM neurons *in vitro*<sup>36</sup>. We found that DLM neurons generated high tonic discharge events (>250 Hz) from high baseline firing rates (~100 Hz), and these events did not exhibit refractory periods (**Supplementary Fig. 1**). Finally, DLM neurons exhibited song-locked rate modulations following lesion of pallidal inputs (**Fig. 3**). Thus, although our results do not rule out a possible role for low threshold calcium channels, they suggest that song-locked signals in DLM do not require inhibitory pallidal inputs and therefore do not require a post-inhibitory rebound mechanism.

A second possible explanation for the paradoxical coactivations observed in pallidal and thalamic neurons arises from the fact that pallidal and thalamic neurons were previously only recorded separately during behavior. Thus, it was not known whether activated pallidal and thalamic neurons were synaptically connected, or rather were recorded from different channels of the basal ganglia–thalamic circuit<sup>38</sup>. In this scenario, pallidal neurons that exhibit rate increases at movement onset could effectively suppress some thalamic neurons, whereas pallidal neurons in a different channel could simultaneously exhibit rate decreases that, through disinhibition, activate other thalamic neurons<sup>3,38,39</sup>. In the absence of information about the synaptic connectivity of these neurons, the activated pallidal and activated thalamic neurons might be interpreted as showing paradoxical coactivation when in fact there is no actual coactivation in a single basal ganglia–thalamic channel.

By recording from connected pallidal and thalamic neurons during vocal babbling, we found that pallidal and thalamic coactivations can occur in the same basal ganglia–thalamic channel. Our data suggest that this occurs because thalamic activity is driven by excitatory cortical inputs that oppose the temporally matched inhibitory inputs from the basal ganglia. This tendency of pallidal and RA<sub>DLM</sub> neurons to exhibit similar firing patterns during singing could result from their common inputs from HVC, a hypothesis that could be tested by recording from Area X, DLM and RA in HVC-lesioned birds. Notably, similar excitation–inhibition matching has been observed in cortex and has been suggested to be involved in temporal gating of sensory inputs<sup>40,41</sup>.

Although our data suggest that cortical inputs to thalamus are important, we also found that basal ganglia outputs have a substantial effect on thalamic activity. Consistent with the inhibitory nature of the pallidothalamic synapse<sup>4,10,13,18–20,27</sup>, the activities of synaptically connected pallidal and DLM neurons were strongly anti-correlated during singing: pallidal rate increases were associated with thalamic rate decreases, and vice versa, even at syllable onsets (**Fig. 2g–k** and **Supplementary Fig. 8**). In addition, consistent with a role for pallidal inputs in controlling thalamic spike timing<sup>20,36</sup>, DLM spikes were entrained to preceding pallidal spikes with submillisecond precision (**Fig. 2d–f**). These findings clearly demonstrate that pallidal inputs are important modulators of thalamic activity during behavior. However, pallidal modulation of thalamic activity does not appear necessary for aspects of thalamic motor function, as thalamic premotor signals persisted following lesion of basal ganglia inputs (**Fig. 3**), and basal ganglia lesions in juvenile and adult birds have little, if any, immediate effect on song structure<sup>15,17</sup>.

What, then, are the functions of the songbird basal ganglia<sup>42</sup>? Area X lesions result in protracted song variability and poor imitation<sup>15</sup>, but the reasons for this remain unclear. We suggest two possible explanations. First, LMAN driven variability is biased in such a way as to reduce vocal errors<sup>43,44</sup>, and the song-locked pallidal

rate modulations observed in this and a previous study<sup>22</sup> may be involved in biasing variability to drive learning<sup>45</sup>. Second, pallidal control of thalamic spike timing could be involved in regulating spike timing–plasticity to direct learning in downstream motor cortical circuits<sup>46,47</sup>.

In summary, although pallidal inputs clearly produce large modulations in thalamic firing rates, we found that cortical inputs may act as principle drivers of behavior-locked activity in the thalamus<sup>12</sup>. We recently found that vocal babbling requires two cortical areas (RA and LMAN), as well as the basal ganglia–recipient thalamus (DLM) that interconnects them, but not the basal ganglia itself<sup>16,17</sup>. Our results support the idea that the basal ganglia–recipient thalamus mediates interactions between cortical areas that are important for behavior<sup>21</sup>. For example, RA, DLM and LMAN could form a reverberant cortico-thalamocortical loop that generates vocal babbling. In addition, corticothalamic signals may be involved in driving learning in cortical circuits. In particular, signals transmitted from RA to DLM could be involved in the early development of stereotyped vocal structure in the songbird<sup>25,26</sup> or in the biasing of motor output toward improved behavioral performance during learning<sup>43–45</sup>. Because songbird cortical areas differ from mammalian cortex in several ways<sup>48,49</sup>, it will be necessary to test whether corticothalamic projections in mammals have a similar role in driving basal ganglia–recipient thalamus during exploratory behavior and learning.

## METHODS

Methods and any associated references are available in the online version of the paper at <http://www.nature.com/natureneuroscience/>.

*Note: Supplementary information is available on the Nature Neuroscience website.*

## ACKNOWLEDGMENTS

We thank A. Graybiel and M. Farries for comments on the manuscript. This work was supported by grants from the US National Institutes of Health (R01DC009183 to M.S.F. and K99NS067062 to J.H.G.), and post-doctoral fellowships from the Charles King Trust and Damon Runyon Research Foundation.

## AUTHOR CONTRIBUTIONS

J.H.G. and M.S.F. designed the experiments and wrote the manuscript. J.H.G. conducted the experiments.

## COMPETING FINANCIAL INTERESTS

The authors declare no competing financial interests.

Published online at <http://www.nature.com/natureneuroscience/>.

Reprints and permissions information is available online at <http://www.nature.com/reprints/index.html>.

- Graybiel, A.M. The basal ganglia: learning new tricks and loving it. *Curr. Opin. Neurobiol.* **15**, 638–644 (2005).
- Reiner, A. You cannot have a vertebrate brain without a basal ganglia. in *The Basal Ganglia IX* (eds. Groenewegen, H.J., Voorn, P., Berendse, H.W., Mulder, A.B. & Cools, A.R.) 3–24 (Springer, New York, 2009).
- Hikosaka, O. GABAergic output of the basal ganglia. *Prog. Brain Res.* **160**, 209–226 (2007).
- Chevalier, G. & Deniau, J.M. Disinhibition as a basic process in the expression of striatal functions. *Trends Neurosci.* **13**, 277–280 (1990).
- DeLong, M.R. Primate models of movement disorders of basal ganglia origin. *Trends Neurosci.* **13**, 281–285 (1990).
- Kultas-Ilinsky, K., Sivan-Loukianova, E. & Ilinsky, I.A. Reevaluation of the primary motor cortex connections with the thalamus in primates. *J. Comp. Neurol.* **457**, 133–158 (2003).
- Albin, R.L., Young, A.B. & Penney, J.B. The functional anatomy of basal ganglia disorders. *Trends Neurosci.* **12**, 366–375 (1989).
- Strick, P.L. Activity of ventrolateral thalamic neurons during arm movement. *J. Neurophysiol.* **39**, 1032–1044 (1976).
- Anderson, M.E. & Turner, R.S. Activity of neurons in cerebellar-receiving and pallidal-receiving areas of the thalamus of the behaving monkey. *J. Neurophysiol.* **66**, 879–893 (1991).

10. Inase, M., Buford, J.A. & Anderson, M.E. Changes in the control of arm position, movement, and thalamic discharge during local inactivation in the globus pallidus of the monkey. *J. Neurophysiol.* **75**, 1087–1104 (1996).
11. Deniau, J.M., Lackner, D. & Feger, J. Effect of substantia nigra stimulation on identified neurons in the VL–VA thalamic complex: comparison between intact and chronically decorticated cats. *Brain Res.* **145**, 27–35 (1978).
12. Sherman, S.M. & Guillery, R.W. *Exploring the Thalamus and Its Role in Cortical Function* (MIT Press, Cambridge, Massachusetts, USA, 2006).
13. Kunimatsu, J. & Tanaka, M. Roles of the primate motor thalamus in the generation of antisaccades. *J. Neurosci.* **30**, 5108–5117 (2010).
14. Bottjer, S.W., Miesner, E.A. & Arnold, A.P. Forebrain lesions disrupt development but not maintenance of song in passerine birds. *Science* **224**, 901–903 (1984).
15. Scharff, C. & Nottebohm, F. A comparative study of the behavioral deficits following lesions of various parts of the zebra finch song system: implications for vocal learning. *J. Neurosci.* **11**, 2896–2913 (1991).
16. Aronov, D., Andalman, A.S. & Fee, M.S. A specialized forebrain circuit for vocal babbling in the juvenile songbird. *Science* **320**, 630–634 (2008).
17. Goldberg, J.H. & Fee, M.S. Vocal babbling in songbirds requires the basal ganglia-recipient motor thalamus but not the basal ganglia. *J. Neurophysiol.* **105**, 2729–2739 (2011).
18. Person, A.L. & Perkel, D.J. Pallidal neuron activity increases during sensory relay through thalamus in a songbird circuit essential for learning. *J. Neurosci.* **27**, 8687–8698 (2007).
19. Kojima, S. & Doupe, A.J. Activity propagation in an avian basal ganglia-thalamocortical circuit essential for vocal learning. *J. Neurosci.* **29**, 4782–4793 (2009).
20. Leblois, A., Bodor, A.L., Person, A.L. & Perkel, D.J. Millisecond timescale disinhibition mediates fast information transmission through an avian basal ganglia loop. *J. Neurosci.* **29**, 15420–15433 (2009).
21. McFarland, N.R. & Haber, S.N. Thalamic relay nuclei of the basal ganglia form both reciprocal and nonreciprocal cortical connections, linking multiple frontal cortical areas. *J. Neurosci.* **22**, 8117–8132 (2002).
22. Goldberg, J.H., Adler, A., Bergman, H. & Fee, M.S. Singing-related neural activity distinguishes two putative pallidal cell types in the songbird basal ganglia: comparison to the primate internal and external pallidal segments. *J. Neurosci.* **30**, 7088–7098 (2010).
23. Llinas, R.R. & Steriade, M. Bursting of thalamic neurons and states of vigilance. *J. Neurophysiol.* **95**, 3297–3308 (2006).
24. Jeanmonod, D., Magnin, M. & Morel, A. Low-threshold calcium spike bursts in the human thalamus. Common physiopathology for sensory, motor and limbic positive symptoms. *Brain* **119**, 363–375 (1996).
25. Veit, L., Aronov, D. & Fee, M.S. Learning to breathe and sing: development of respiratory-vocal coordination in young songbirds. *J. Neurophysiol.* **106**, 1747–1765 (2011).
26. Aronov, D., Veit, L., Goldberg, J.H. & Fee, M.S. Two distinct modes of forebrain circuit dynamics underlie temporal patterning in the vocalizations of young songbirds. *J. Neurosci.* **31**, 16353–16368 (2011).
27. Luo, M. & Perkel, D.J.A. GABAergic, strongly inhibitory projection to a thalamic nucleus in the zebra finch song system. *J. Neurosci.* **19**, 6700–6711 (1999).
28. Wild, J.M. Descending projections of the songbird nucleus robustus archistriatalis. *J. Comp. Neurol.* **338**, 225–241 (1993).
29. Vates, G.E., Vicario, D.S. & Nottebohm, F. Reafferent thalamo-“cortical” loops in the song system of oscine songbirds. *J. Comp. Neurol.* **380**, 275–290 (1997).
30. Georgopoulos, A.P., DeLong, M.R. & Crutcher, M.D. Relations between parameters of step-tracking movements and single cell discharge in the globus pallidus and subthalamic nucleus of the behaving monkey. *J. Neurosci.* **3**, 1586–1598 (1983).
31. Anderson, M.E. & Horak, F.B. Influence of the globus pallidus on arm movements in monkeys. III. Timing of movement-related information. *J. Neurophysiol.* **54**, 433–448 (1985).
32. Anderson, M.E. & Turner, R.S. A quantitative analysis of pallidal discharge during targeted reaching movement in the monkey. *Exp. Brain Res.* **86**, 623–632 (1991).
33. Yoshida, A. & Tanaka, M. Enhanced modulation of neuronal activity during antisaccades in the primate globus pallidus. *Cereb. Cortex* **19**, 206–217 (2009).
34. Sheth, S.A., Abuelem, T., Gale, J.T. & Eskandar, E.N. Basal ganglia neurons dynamically facilitate exploration during associative learning. *J. Neurosci.* **31**, 4878–4885 (2011).
35. Pare, D., Curro'Dossi, R. & Steriade, M. Neuronal basis of the parkinsonian resting tremor: a hypothesis and its implications for treatment. *Neuroscience* **35**, 217–226 (1990).
36. Person, A.L. & Perkel, D.J. Unitary IPSPs drive precise thalamic spiking in a circuit required for learning. *Neuron* **46**, 129–140 (2005).
37. Coulter, D.A., Huguenard, J.R. & Prince, D.A. Calcium currents in rat thalamocortical relay neurons: kinetic properties of the transient, low-threshold current. *J. Physiol. (Lond.)* **414**, 587–604 (1989).
38. Mink, J.W. The basal ganglia: focused selection and inhibition of competing motor programs. *Prog. Neurobiol.* **50**, 381–425 (1996).
39. Deniau, J.M. & Chevalier, G. Disinhibition as a basic process in the expression of striatal functions. II. The striato-nigral influence on thalamocortical cells of the ventromedial thalamic nucleus. *Brain Res.* **334**, 227–233 (1985).
40. Okun, M. & Lampl, I. Instantaneous correlation of excitation and inhibition during ongoing and sensory-evoked activities. *Nat. Neurosci.* **11**, 535–537 (2008).
41. Vogels, T.P. & Abbott, L.F. Gating multiple signals through detailed balance of excitation and inhibition in spiking networks. *Nat. Neurosci.* **12**, 483–491 (2009).
42. Doupe, A.J., Perkel, D.J., Reiner, A. & Stern, E.A. Birdbrains could teach basal ganglia research a new song. *Trends Neurosci.* **28**, 353–363 (2005).
43. Andalman, A.S. & Fee, M.S. A basal ganglia-forebrain circuit in the songbird biases motor output to avoid vocal errors. *Proc. Natl. Acad. Sci. USA* **106**, 12518–12523 (2009).
44. Warren, T.L., Tumer, E.C., Charlesworth, J.D. & Brainard, M.S. Mechanisms and time course of vocal learning and consolidation in the adult songbird. *J. Neurophysiol.* **106**, 1806–1821 (2011).
45. Fee, M.S. & Goldberg, J.H. A hypothesis for basal ganglia-dependent reinforcement learning in the songbird. *Neuroscience* **198**, 152–170 (2011).
46. Markram, H., Lubke, J., Frotscher, M. & Sakmann, B. Regulation of synaptic efficacy by coincidence of postsynaptic APs and EPSPs. *Science* **275**, 213–215 (1997).
47. Pasupathy, A. & Miller, E.K. Different time courses of learning-related activity in the prefrontal cortex and striatum. *Nature* **433**, 873–876 (2005).
48. Jarvis, E.D. Learned birdsong and the neurobiology of human language. *Ann. NY Acad. Sci.* **1016**, 749–777 (2004).
49. Butler, A.B., Reiner, A. & Karten, H.J. Evolution of the amniote pallium and the origins of mammalian neocortex. *Ann. NY Acad. Sci.* **1225**, 14–27 (2011).



## ONLINE METHODS

**Animals.** We used juvenile male zebra finches ( $n = 26$ ) at the subsong stage of song development (36–55 dph) and one additional young adult (110 dph) singing undirected song for our experiments. Excitotoxic lesions to Area X were performed in an additional three birds (50–60 dph) as described below. Birds were obtained from the Massachusetts Institute of Technology zebra finch breeding facility. The care and experimental manipulation of the animals were carried out in accordance with guidelines of the US National Institutes of Health and were reviewed and approved by the Massachusetts Institute of Technology Committee on Animal Care.

**Chronic neural recordings and histology.** Using motorized microdrives for chronic neural recordings, electrodes were implanted into DLM ( $n = 11$  birds), RA ( $n = 5$  birds) or Area X ( $n = 4$  birds), and recordings were carried out as described previously<sup>22</sup>. Units accepted for analysis had signal-to-noise ratios (average spike peak amplitude compared with s.d. of noise) of  $>10:1$ . Antidromic identification of LMAN-projecting DLM neurons and DLM-projecting RA neurons was carried out with a bipolar stimulating electrode implanted in LMAN or DLM using techniques described previously (stimulation intensities, 50–300  $\mu\text{A}$  for 200  $\mu\text{s}$ ). All of the antidromically identified DLM and RA neurons in our dataset were further validated with collision tests. At the conclusion of the experiments, small electrolytic lesions (20  $\mu\text{A}$  for 15 s) were made through the recording and stimulation electrodes for histological verification of electrode positions. Of the 29 DLM neurons, 17 were antidromically identified and collision tested. The other 12 neurons did not respond to LMAN stimulation with a short-latency spike, but did exhibit spike waveforms, firing patterns and correlations to song temporal structure similar to the identified projection neurons and were included in the analysis. We suspect that these were LMAN-projecting DLM neurons, but that they did not project to the part of LMAN activated by the stimulation electrode in DLM. Of 115 neurons recorded in RA, 17 were antidromically identified and collision tested as DLM-projecting.

RA neurons terminate in both DLM and the nearby dorsomedial thalamic nucleus (DMP), just posterior and medial to DLM<sup>50</sup> (Fig. 4e–h and Supplementary Fig. 9). This raises the possibility that our antidromic stimulating electrode in DLM may activate not just fibers that terminate in DLM, but also those that terminate in DMP. We observed single RA axons branching and coursing through both DLM and DMP (Supplementary Fig. 9), suggesting that some individual RA neurons may project to both DLM and DMP. However, if there are neurons that project only to DMP, we cannot rule out the possibility that our antidromic stimulation procedure might identify neurons projecting only to DMP. However, given the homogeneity of firing patterns of thalamus projecting RA neurons, it seems likely that our conclusions about the nature of the signal being transmitted to DLM would be altered by this fact. As a separate issue, it is also possible that some of the neurons that were not antidromically identified may also have been DLM projectors, but these were analyzed separately (Supplementary Fig. 12).

To visualize pallidal terminals and thalamic neurons in DLM (as in Fig. 1c), Alexa Dextran-555 (Molecular Probes) was injected into Area X for anterograde labeling of calyceal terminals and Alexa dextran-647 into LMAN for retrograde labeling of DLM neurons. For DLM tract-tracing experiments (Fig. 4), Alexa Dextran-555 or Cholera toxin beta subunit (Molecular Probes) were injected into DLM, MMAN or LMAN. For anterograde tracing of RA axons terminating in DLM and DMP, herpes virus expressing GFP on a CMV promoter, obtained from the Massachusetts Institute of Technology viral core facility, was injected into RA. We imaged 100- $\mu\text{m}$  brain slices with a Nikon PCM2000 confocal microscope, and ImageJ (US National Institutes of Health) was used to merge serial sections. All histological figures show sagittal sections.

**Targeting DLM.** We targeted the Area X–recipient portion of DLM for recording as follows. Prior to microdrive implantation, the antero-posterior and dorso-ventral extent of this region was determined by electrophysiologically mapping the high-frequency firing, thin-spiking pallidal axon terminals that constitute Area X outputs<sup>18,22</sup>. We have found that the medial zone of the pallidal terminal region did not exhibit singing-related firing patterns. This region likely corresponded to the ventromedial portion of DLM that was not innervated by Area X and that projected to a shell surrounding LMAN<sup>50</sup>. We found that the center of the singing-related Area X–recipient zone was reliably located at 1.07 mm lateral

to the midline. Thus, using a head angle of 65 degrees relative to the flat anterior portion of the skull, electrodes were targeted to the center of Area X recipient portion of DLM: 1.07 mm lateral to midline and, depending on the individual bird, between +0.9–1.5 mm anterior to the bifurcation of the mid-sagittal sinus ( $\lambda$ ), and  $\sim 4.3$  mm ventral to the brain surface. Using this technique, we reliably recorded from LMAN projecting DLM neurons and avoided DMP, a nearby thalamic nucleus where pallidal axon terminals are not observed in extracellular recordings (Supplementary Fig. 11).

**Area X lesion methods and histological confirmation.** Bilateral excitotoxic lesions of Area X were made by injecting 200 nl of 4% *N*-methyl-DL aspartic acid (NMA, Sigma) into the center of each Area X (head angle 20 degrees, 5.8 mm anterior, 1.5 mm lateral and 2.85 mm ventral) and an additional 50 nl into each medial Area X, using stereotactic coordinates (head angle 20 degrees, 5.8 anterior, 1.2 mm lateral, 2.6 mm ventral). Recording and stimulating electrodes were implanted into DLM and LMAN, respectively, immediately following the Area X lesion (during the same surgery). Birds rapidly recovered from the lesion and began singing within 2–4 d. Recordings were acquired from singing birds 5–12 d after the Area X lesion. Previously, this lesion protocol reliably lesioned between 80–100% of Area X ( $n = 19$  birds)<sup>17</sup>. As described previously, lesions were confirmed histochemically using fluorescent antibody to neuronal nuclei (mouse antibody to Neu-N, Millipore); Area X stained brighter than background in Neu-N staining and lesion boundaries were clearly visible<sup>17</sup>. In addition to histological confirmation, Area X lesions were functionally confirmed; although pallidal terminals were always observed in electrode penetrations through DLM of control birds, terminals were never observed in DLM of Area X lesioned birds.

**Statistical analysis.** We represented neural activities as instantaneous firing rates,  $R(t)$ , defined at each time point as the inverse of the enclosing interspike interval

$$R(t) = \frac{1}{t_{i+1} - t_i}, \text{ for } t_i < t \leq t_{i+1}$$

where  $t_i$  is the time of the  $i^{\text{th}}$  spike. Note that IFRs were computed as the inverse of the interspike interval for the duration of that interval and they therefore measured firing rate. Thus, the IFR cross-correlation analysis (as in Fig. 2h) computes the relation between pallidal and thalamic firing rates. In contrast, a standard cross-correlogram analysis (as in Fig. 2f) computes the spiking probability in a temporally defined bin.

**Spike sorting and analysis.** Spikes were sorted offline using custom Matlab software (A. Andalman, D. Aronov, J.F.G. and M.S.F.). DLM spikes were distinguished from pallidal terminals by their wider spike widths, lower mean firing rate during non-singing periods and antidromic activation from LMAN, as previously described<sup>22</sup>. To sort spikes from pairs simultaneously recorded on the same electrode, we developed a template-matching spike sorting algorithm that automatically detected and assigned identity to spike overlaps (Supplementary Fig. 4). HTD events<sup>9</sup> in DLM were defined as firing events exceeding 250 Hz. We tested different thresholds between 200 and 300 Hz; in all cases, HTDs were generated from high levels of background activity. They were more frequent during singing and did not exhibit refractory periods (Supplementary Fig. 1).

**Analysis of correlations of neural activity to song temporal structure.** Neural activity was aligned to the 300 ms preceding and following all syllable onsets and offsets. Only cells recorded for greater than 50 syllables were accepted. To determine the significance of firing rate peaks and troughs, a rate histogram (bin size, 10 ms) was generated of the real data (as in Fig. 1f). A surrogate histogram was then generated in which each trial of syllable-aligned neural activity was time-shifted by a uniformly distributed random amount over a range equal to the duration of the histogram (600 ms). The shift was circular, such that spikes wrapped around to the beginning of the histogram, preserving the overall spike statistics of the data. The minimum and maximum of the surrogate rate histogram was then obtained with 1,000 repetitions of randomly shifted data.  $P$  values for the rate minima and maxima of the real dataset were calculated by analyzing the frequency with which shifted datasets generated larger maxima or smaller minima in firing rates. Peaks and troughs in firing rate with  $P < 0.05$  were considered significant.

The amplitude of the rate modulation was computed as the maximal deviation from the rate from a baseline period of the histogram (−300 to −200 ms before syllable onset or offset). The timing of the rate change relative to the syllable onset (or offset) was computed as the time at which the rate change surpassed two s.d. above (for rate increases) or below (for rate decreases) the baseline rate. Using different criteria for the detection of the rate change, including 1, 3 and 4 s.d. from the mean, did not significantly alter our conclusions.

To construct population rate histograms (as in **Fig. 1g**), we mean-subtracted data from individual cells and then averaged the data across the group. To compute fractional changes in firing rates at the onsets and offsets of syllables and singing epochs (as in **Fig. 6h,i**), we normalized the mean-subtracted rate histogram by the mean rate in the baseline period. Lag cross-correlations for the paired pallidothalamic recordings were computed using the `xcorr` function in Matlab. The significance of the anti-correlation at zero time lag was computed using the `corrcoef` function.

**Assessing the functionality of the RA projection to DLM.** In subsong-aged anesthetized birds ( $n = 9$  birds, 35–49 dph), a bipolar stimulation electrode was implanted in RA and a custom-fabricated reverse microdialysis probe<sup>16</sup>

(**Supplementary Fig. 10**) was implanted in Area X. Recording electrodes were targeted to the Area X-recipient portion of DLM, as described previously<sup>18,22</sup>. Pallidal terminals were recorded as muscimol (1.5 mg ml<sup>−1</sup>) or tetrodotoxin (1 μM) (Sigma-Aldrich) was infused through the dialysis probes. Inactivation of Area X was confirmed by the disappearance of pallidal activity (**Supplementary Fig. 10c**), as described previously<sup>19</sup>. DLM neurons were recorded during either burst stimulation in RA (each burst consisted of 3–5 stimulations at 500 Hz, 200-μs pulse width, 60–150-μA stimulus current, bursts delivered at 0.5 or 1 Hz) or during single-stimulation in RA (single stimulations delivered at 0.5 or 1 Hz, 60–150 μA stimulus current; **Supplementary Fig. 10**). The latency of the DLM response to RA stimulation was computed as the time in the PSTH (bin size, 5 ms) where the rate exceeded 2 s.d. above baseline period of 0.3 s before the stimulation. To assess the significance of the rate change following RA stimulation, we subjected rate histograms to the statistical analysis described above for syllable onsets.

50. Foster, E.F., Mehta, R.P. & Bottjer, S.W. Axonal connections of the medial magnocellular nucleus of the anterior neostriatum in zebra finches. *J. Comp. Neurol.* **382**, 364–381 (1997).